ADVANCED FUNCTIONAL MATERIALS
www.afm-journal.de

Strategies for Integrating Metal Nanoparticles with Two-Photon Polymerization Process: Toward High Resolution Functional Additive Manufacturing

Jisun Im, Yaan Liu, Qin Hu, Gustavo F. Trindade, Christopher Parmenter, Michael Fay, Yinfeng He, Derek J. Irvine, Christopher Tuck, Ricky D. Wildman, Richard Hague,* and Lyudmila Turyanska**

This study reports the successful fabrication of complex 3D metal nanoparticle–polymer nanocomposites using two-photon polymerization (2PP). Three complementary strategies are detailed: in situ formation of metal nanoparticles (MeNPs) through a single-step photoreduction process, integration of pre-formed MeNPs into 2PP resin, and site-selective MeNPs decoration of 3D 2PP structures. In the in situ formation strategy, a phase-transfer method is applied to transfer silver and copper ions from an aqueous phase into a toluene solvent to disperse them in photoreactive monomers. The addition of a photosensitive dye, coumarin 30, facilitated the reduction of silver ions and improved the distribution of silver nanoparticles (AgNPs). This strategy is successfully used to produce other MeNPs, such as Cu and Au. The integration of pre-formed MeNPs enabled highly controlled NP size distribution within the 2PP 3D structures with high-fidelity To enable selective decoration of 2PP 3D surfaces with MeNPs, a multimaterial strategy is developed, with one of the resins designed for thiol-ene reaction, which demonstrated selective binding to AuNPs. The successful development of complementary strategies for integration of MeNPs into 2PP resins offers exciting opportunities for fabrication of MeNP composites with sub-micron resolution for applications from photonics to metamaterials and drug delivery.

1. Introduction

There is an increasing demand for 3D micro/nano-fabrication in a variety of applications, including nanophotonics, micro-electromechanical systems, microelectronics, microfluidics, and tissue engineering and drug delivery.[1–3] It has been proposed that the limitations of traditional manufacturing (e.g. lithography) for the fabrication of 3D microstructures could be overcome by multiphoton additive manufacturing (AM) processes,[4,5] such as femtosecond laser-induced two-photon polymerization (2PP). These techniques offer opportunities for fabrication of 3D structures with nanoscale resolution, high degrees of design freedom, and comparably fast build speed.[6–8] However, the availability of functional materials that are suitable for use in these processes is scarce, leading to limited exploitation of these technologies.

More specifically to this study, the ability to fabricate nanoscale 3D structures containing metal nanoparticles (MeNPs) can enable advances in a range of applications from plasmonics and metamaterials to biosensors.[9–12] Hence, integration of MeNPs into 3D micro/nano-scale structures without disturbing the quality and resolution of the 2PP processes has attracted considerable attention. Previously, the direct photoreduction of a metal salt for the in situ formation of metal structures has been reported for

J. Im, Y. Liu, Q. Hu, G. F. Trindade, Y. He, D. J. Irvine, C. Tuck, R. D. Wildman, R. Hague, L. Turyanska
Centre for Additive Manufacturing
Faculty of Engineering
University of Nottingham
Jubilee Campus
Nottingham NG7 2RD, UK
E-mail: Ricky.Wildman@nottingham.ac.uk;
Richard.Hague@nottingham.ac.uk;
Lyudmila.Turyanska@nottingham.ac.uk

The ORCID identification number(s) for the author(s) of this article can be found under https://doi.org/10.1002/adfm.202211920.

DOI: 10.1002/adfm.202211920

G. F. Trindade
National Physical Laboratory
Teddington, Middlesex TW11 0LW, UK

C. Parmenter, M. Fay
Nanoscale and Microscale Research Centre
University of Nottingham
Nottingham NG7 2RD, UK

Y. He
Nottingham Ningbo China Beacons of Excellence
Research and Innovation Institute
No. 211, Xinguang Road, Ningbo 315101, China

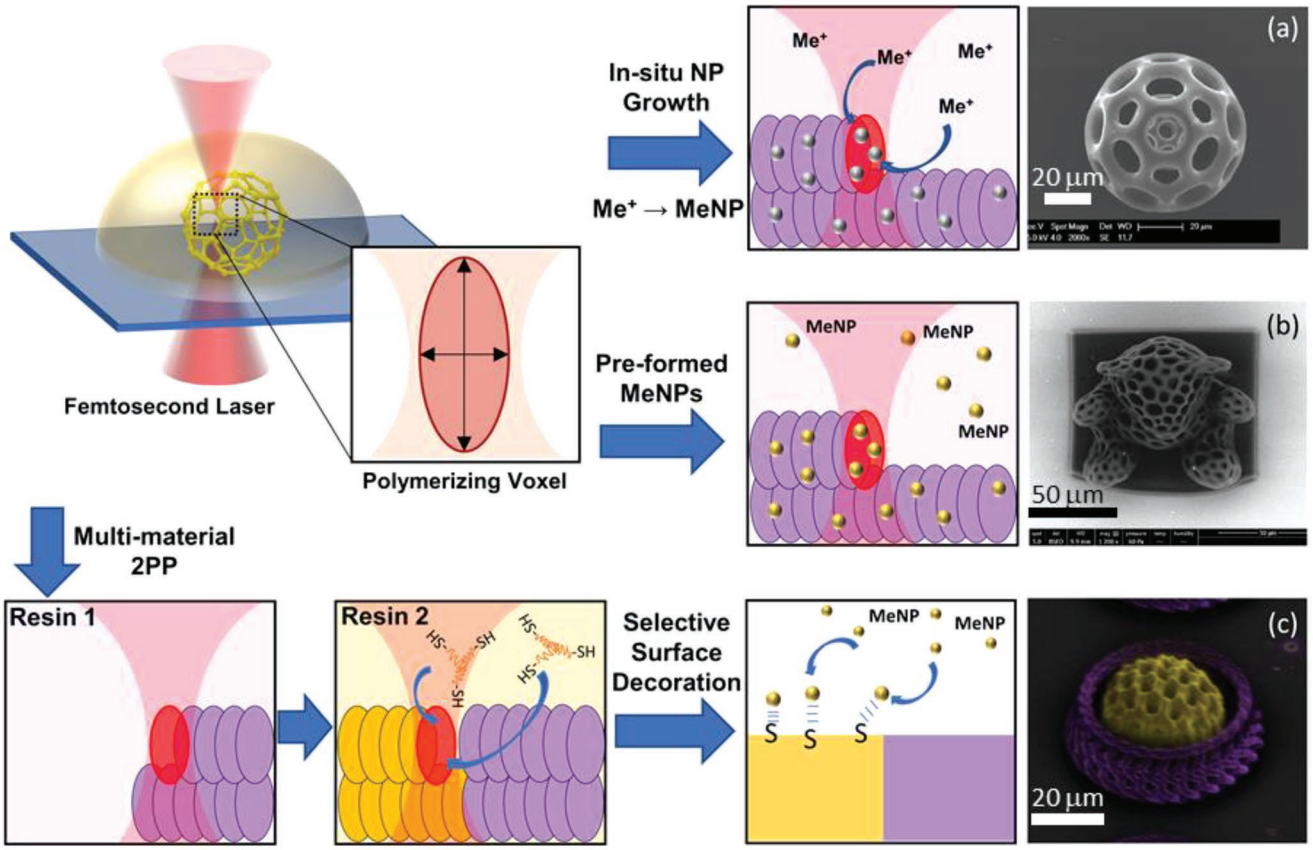

Figure 1. Schematic diagram of the three strategies for integration of metal nanoparticles (MeNPs) with 2PP process and representative SEM images of the 3D 2PP microstructures produced using a) in situ NP growth method and b) the resin with pre-formed NPs, and c) ToF-SIMS mapping image of a multimaterial structure for selective surface decoration with NPs (yellow and purple colors indicate the parts decorated with AuNPs and PETA polymer, respectively).

gold nanoparticles (AuNPs),[13–15] and conductive silver nanowires and micropillars.[16,17] Resins containing pre-fabricated gold nanorods[18,19] as well as gold-crosslinked polymer composites[20,21] have also been used for 2PP processes to form solid microstructure aggregates and micro/nanostructures. However, these methods often require post-fabrication processing[16,17] and provide limited control of the nanoparticle size and location. Despite significant interest, the integration of MeNPs, such as noble metals and copper nanoparticles (CuNPs), with 2PP processes remains challenging. This is due to several factors, such as solubility of metal salts in solvents compatible with 2PP and the interaction of the laser beam with nanofillers that can lead to lowering of the printing resolution. Even where successes were reported,[15] narrow size distribution of the nanoparticles and control of their position have not been achieved yet. Hence, to address the diverse requirements for different applications, there is a strong need for the development of robust strategies to enable integration of different MeNPs, control of their size distribution, and selective deposition for patterning of the 3D structures.

In this paper, we propose three complementary strategies for integration of MeNPs with 2PP processes: a) in situ growth of MeNPs, b) integration of pre-formed NPs, and c) selective surface decoration of functionalized multimaterial structures (**Figure 1**). We successfully demonstrate that in situ metal reduction can be successfully applied to integrate different metals, such as Ag and Cu, into 2PP structures. In this case, simultaneous photopolymerization and photoreduction processes enable the formation of large densities of MeNPs (up to $\approx 10^3$ NPs per voxel) during printing, although the control of size distribution can be challenging. Meanwhile, we report the narrow size distribution with controlled MeNP size by demonstrating, for the first time, 2PP with resins that include pre-formed MeNPs. Using this strategy, MeNP containing (6 NPs per voxel) 2PP structures with high fidelity and resolution were produced by optimizing the properties of the NPs to limit any interference with the laser beam and modifying the resin composition to include thiol-functionality. For applications requiring selective surface decoration, we developed a multimaterial 2PP methodology, where one of the resins contains a thiol (i.e., organosulfur compound R–SH, where R represents an alkyl or other organic substituents) to generate binding via the sulphur moiety to MeNPs. For all three strategies developed in this work, we provide detailed morphological and compositional analysis, including advanced ToF-SIMS mapping results, and discuss their benefits for potential applications. Thus, our work addresses key current challenges for 2PP processing by enabling high-resolution sub-micron scale AM of functional materials, which could advance their exploitation in functional devices.

2. Results and Discussion

2.1. In Situ Growth of MeNPs in 2PP Process

For in situ growth of MeNPs, we adopt a simultaneous photoreduction and photopolymerization approach that we had previously successfully demonstrated with gold(III) chloride salts to form AuNPs.[15] However, silver and copper salts, especially the commonly used silver nitrate, have poor solubility in pentaerythritol triacrylate (PETA)-based 2PP resin. In this work, we address the solubility issues by employing a phase-transfer protocol to produce MeNP within the 2PP resin using simultaneous photoreduction and polymerization processes.

A number of PETA-based resins were formulated with different concentrations of photoinitiator (PI) and metal salt (see **Table 1**). As metal salts commonly used for the NP synthesis (e.g., silver nitrate) are typically insoluble in organic solvents, we adopt a phase transfer method to disperse them in PETA. This involved mixing an aqueous solution of a metal salt (e.g., silver nitrate) with an ethanol solution of dodecylamine (DDA).[22] This leads to the formation of Ag or Cu-DDA organometallic complexes, which are extracted into a toluene phase and then mixed with the monomer to form the resin (see detailed method description in Experimental Section and Figure S1 Supporting Information). The DDA/ethanol-toluene-based phase transfer enables us to achieve the concentration of metal ions needed to successfully form MeNPs.

The presence of metal complexes in the resin can affect the photopolymerization and influence the size of the printing window. Hence, to optimize the printing parameters, single lines were printed onto a glass substrate using resins with Irgacure 369 as the PI in varying concentrations up to 5%. For PETA, the threshold laser power (power required to initiate polymerization) was found to decrease with increasing PI concentration from 25 mW for 1% to 17 mW for 5%. This was accompanied by an increase of the linewidth from 319 ± 11 to 386 ± 20 nm for 1% and 5% Irgacure 369, respectively (Figure S2, Supporting Information). The linewidth was found to increase further with the addition of silver ions (molar ratio of PETA:Ag = 5:1), from 386 ± 20 to 605 ± 16 nm for 1% and 3% Irgacure 369, respectively.

Table 1. Composition of 10 formulations for in situ growth of MeNPs in PETA monomer.

Formulation Molar ratio $PETA:Me^{+} = 5:1$	PETA [wt.%]	Irgacure 369 [wt.%]	Coumarin 30 [wt.%]
Irgacure1%-PETA	99	1	
Irgacure1%-PETA-Ag	99	1	
Irgacure1%-PETA-Coumarin-Ag	98.9	1	0.1
Irgacure 3%-PETA	97	3	
Irgacure 3%-Ag	97	3	
Irgacure 3%-Coumarin-Ag	96.9	3	0.1
Irgacure5%-PETA	95	5	
Irgacure5%-PETA-Ag	95	5	
Irgacure5%-PETA-Coumarin-Ag	94.9	5	0.1
Irgacure5%-PETA-Coumarin-Cu	94.9	5	0.1

We found that the addition of 0.1% coumarin 30 dye slightly decreased the required threshold laser power (from 25 ± 1 to 20 ± 1 mW for 1% Irgacure 369), which was accompanied by a decrease of the linewidth, e.g. the linewidth of Ag composite decreased by over 50 nm to reach the value of 547 ± 11 nm (Figure S2, Supporting Information). This was attributed to the excitation of coumarin 30 by the laser. Furthermore, Raman spectroscopy (Figure S3, Supporting Information) revealed an increase of the degree of vinyl group consumption (*DC*) from 27 ± 3% to 43 ± 1% with increasing PI concentration from 1% to 5%, which is comparable to previous reports.[23] Addition of the Ag-salt (molar ratio of PETA:Ag=5:1) affected the polymerization with *DC* = 58 ± 4% for 1% Irgacure 369 increasing to *DC* = 71 ± 1% for 5% Irgacure 369. The addition of coumarin 30 dye did not have a noticeable effect on the *DC* value.

The composition of the resin described above was formulated to enable in situ growth of MeNPs. The coumarin 30 was added to facilitate the photoinduced metal reduction process by electron transfer from the excited dye to silver ions,[24,25] formation of nucleation sites,[26] and surface reduction growth, resulting in formation of larger particles with narrower size distribution. A number of 2D and 3D structures were fabricated with high spatial resolution using these formulations. For example, 3D structures and arrays were successfully fabricated using the Ag-containing resin and 0.1% coumarin 30 dye (**Figure 2**; Figure S4, Supporting Information).

Scanning electron microscopy (SEM) images of these structures (Figure 2c; Figure S5, Supporting Information) revealed the presence of AgNPs on the surface, confirming that successful simultaneous 2PP and photoreduction processing had been achieved. Analysis of cross section transmission electron microscope (TEM) images and EDX studies further confirmed the presence of spherical AgNPs (Figure S6, Supporting Information) with an average size of 5.0 ± 1.0 nm, and a few larger particles (≈60 nm) randomly distributed throughout the volume of the structure (Figure 2d). No significant difference in the NP size was observed in the structures produced with different Ag loading. The addition of coumarin 30 facilitated the formation of slightly larger particles with diameter of 5.8 ± 1.5 nm that were more uniformly distributed throughout the volume of the structures. Additionally, the successful reduction of silver ions was confirmed by the observation of a clear Ag3d peak in X-ray photoelectron spectroscopy (XPS) spectrum, which is characteristic of Ag^0 and Ag_2O (Figure 2e; Table S1, Supporting Information).

To illustrate that the simultaneous photopolymerization and photoreduction strategy could be applied to different metals, copper salts (5%) were also used in resin formulations containing coumarin 30. Similar to the Ag-containing formulations, 2D and 3D structures were also achieved with high fidelity (**Figure 3**a).

ToF-SIMS (time-of-flight secondary ion mass spectrometry) imaging suggested that the CuNPs are aggregated into 5–100 μm sized clusters, with smaller individual particles scattered across the surface (Figure 3b; Figure S7, Supporting Information). The successful in situ growth of MeNPs within the 3D micro/nanostructures demonstrated here offers opportunities

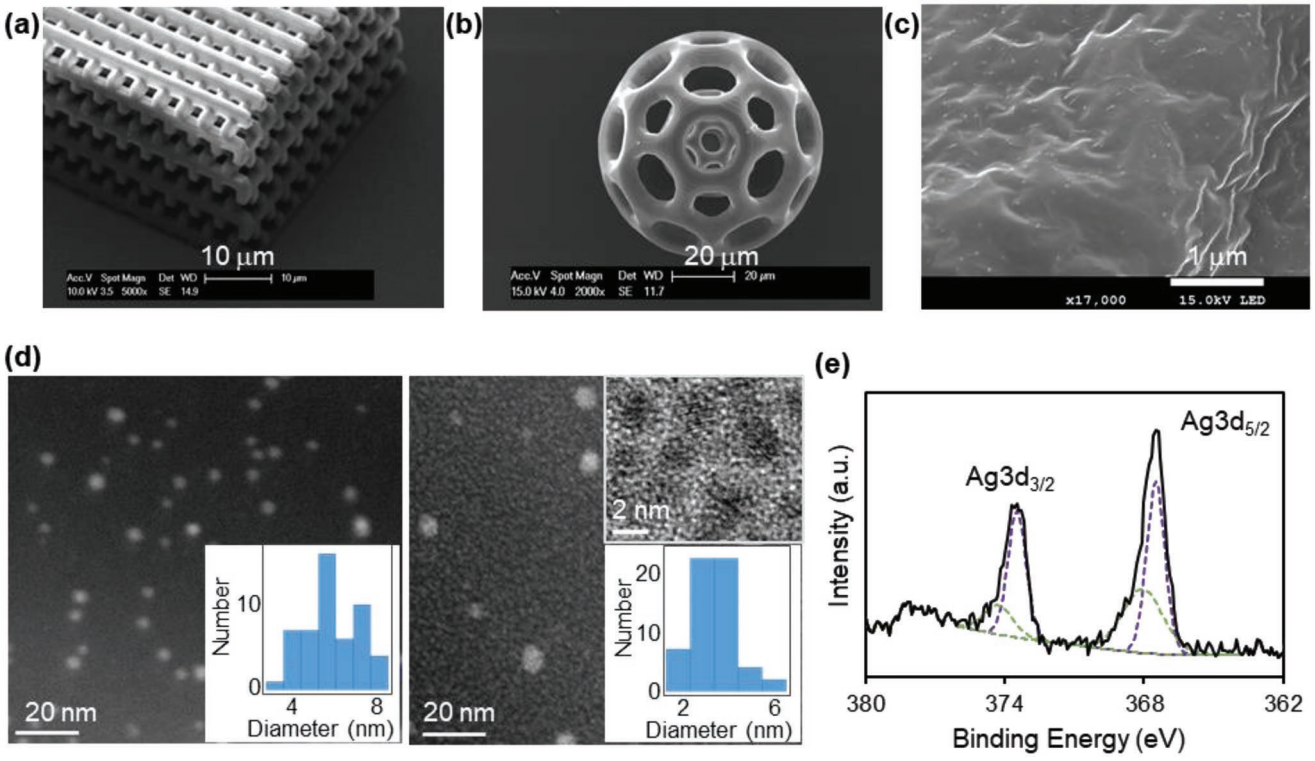

Figure 2. SEM images of PETA-AgNP a) woodpile structure and b) hollow sphere produced with the formulation containing 5% Irgacure 369 and 0.1% coumarin (printing parameters: 10 mW and 10 mm s^{-1}). c) A representative FEG-SEM image of the hollow sphere structure shown in part (b). d) Dark field STEM images showing the presence of AgNPs in the cross sections of the structures fabricated using the formulations (left) without and (right) with 0.1% coumarin and (insets) corresponding histograms of NP size distribution (printing parameters: 15 mW and 10 mm s^{-1}). (Top right inset) A representative high-resolution TEM image of AgNPs produced in situ with 0.1% coumarin. e) Ag3d core level of XPS spectrum of PETA-AgNP structure produced with the formulation containing 5% Irgacure 369 and 0.1% coumarin. The fitted curves represent Ag3d for Ag_2O (purple) and Ag^0 (green), respectively.

for integration of different MeNPs within the 2PP structures, where the NP density is tuneable by the resin composition. However, this study demonstrated that there was limited control of the size distribution of the MeNPs generated within a polymer matrix. Therefore, methods to directly incorporate preformed MeNPs with well-controlled size and distribution were explored.

2.2. 2PP with Preformed MeNPs Dispersed within the Resins

We propose that preformed NPs can be mixed into the photoreactive monomers for 2PP process, provided that the following factors affecting laser focusing are considered: i) the resin must exhibit sufficient transparency at the wavelength of the used laser (780 nm), ii) the oil immersion systems must be refractive

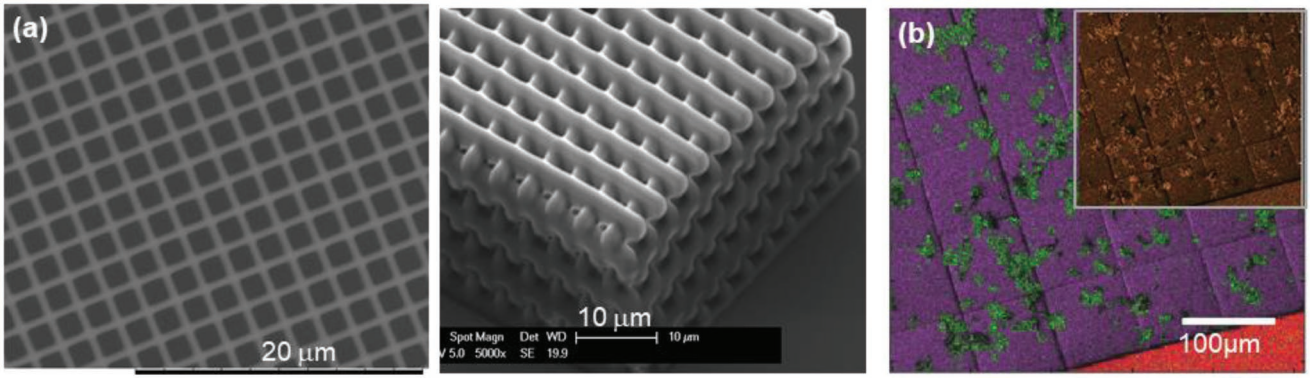

Figure 3. a) 2D and 3D copper-polymer structures fabricated using the formulation containing 5% copper salt and 0.1% coumarin 30 through simultaneous photoreduction and photopolymerization. (printing parameters: 15 mW and 10 mm s^{-1}). b) Representative ToF-SIMS mapping image and (inset) corresponding optical image of a 2PP structure consisting of fifty 100 × 100 × 5 µm squares. ToF-SIMS image reveals the location of copper particles (green, Cu^+ signal) on the surface of the printed polymer matrix (purple, $C_3H_3O^+$ signal). Substrate is indicated in red color (SiO^+ signal).

index matched and iii) the potential effect of NPs on laser light scattering must be prevented. AuNPs with an average diameter of 3 ± 1 nm satisfied these requirements and were chosen for this work (Figure S8, Supporting Information).

Two sets of resin formulations containing different concentrations of AuNPs were prepared. The first, Au-PETA, contained PETA with 7-diethylamino-3-thenoylcoumarin (DETC) as PI and AuNPs. The second resin, Au-thiol-ene, contained the same PETA/DETC/AuNPs blend to which the trifunctional thiol (TrisSH) was added. It was determined that up to 1 wt.% of AuNPs can be homogeneously dispersed in the Au-thiol-ene formulation, due to the interaction between thiols and AuNPs. Meanwhile, with the Au-PETA resin, NP agglomeration was noticeable at the much lower AuNP concentration of ≈0.01 wt.%. Under exposure to laser light (>40 mW), formulations containing AuNPs (concentration ≥ 0.01 wt.%) presented vigorous bubbling due to the NP induced photothermal effects, leading to excessive localized heat and resulting in vaporization or "burning" of the resins.[27]

To establish the effect of NPs on printing resolution, woodpile structures of 50 × 50 μm^2 (5 layers with a line space of 3 μm in *xy*-direction and an interlayer period of 800 nm in *z*-direction) were printed with varying laser powers in the range 5–50 mW and scan speeds between 10 and 21 mm s^{-1}. The printing parameters are used to calculate the value of energy density, *E* (see Experimental Section). Analysis of the SEM images (**Figure 4**; Figure S9, Supporting Information) revealed a lower polymerization threshold for the Au-thiol-ene resins (10 mW, 21 mm s^{-1}, 48 μJ μm^{-3}) compared to the Au-PETA equivalent (40 mW, 21 mm s^{-1}, 190 μJ μm^{-3}). We find that the presence of AuNP in PETA greatly affects the PETA processing window and the fidelity of the designed structures. Instead, for thiol-ene resin, the fidelity and resolution of the printed structures produced with and without the AuNPs are comparable. The polymerization rate of acrylate resin can be accelerated by the addition of thiols due to the reduced oxygen inhibition in thiol-acrylate photopolymerization process. In free radical polymerization of acrylates, oxygen dissolved in the resin can lead to the formation of peroxy radicals and thus chain termination. With addition of thiols, peroxy radicals can abstract the thiol hydrogen to generate thiyl radicals that can continue to propagate through addition or chain transfer.[28–30] This leads to a wider printing window with a lower polymerization threshold for Au-thiol-ene resin compared to Au-PETA resin. Optimal parameters were found to be within the energy density range of 48–100μJμm^{-3} (10–21 mm s^{-1} at 10 mW) for Au-thiol-ene resins and 214–450 μJ μm^{-3} (10–21 mm s^{-1} at 45 mW and 13–21 mm s^{-1} at 50 mW) for Au-PETA.

Cross section TEM analysis revealed the presence of AuNP with diameter of 3 ± 1 nm (Figure 4d), indicating that the 2PP process does not alter the NP morphology. The high-angle annular dark-field (HAADF) images were used to estimate the number of AuNPs per cross section area that is equal to the voxel size (lateral length: 200 nm, axial length: 500 nm, aspect ratio: 2.5).[31] On average, 6 AuNPs were found per voxel in Au-thiol-ene structures (Figure 4e), which is close to the estimate based on the assumption that the added NPs are uniformly distributed throughout the resin (5 AuNPs per voxel for 0.01 wt.% AuNP formulation). We note that no AuNPs were detected in the cross section TEM images acquired for Au-PETA resin structures. This suggested a dominant role of the host matrix interaction with the NPs in defining the level of NP integration into the resin that can be achieved during the photopolymerization process.

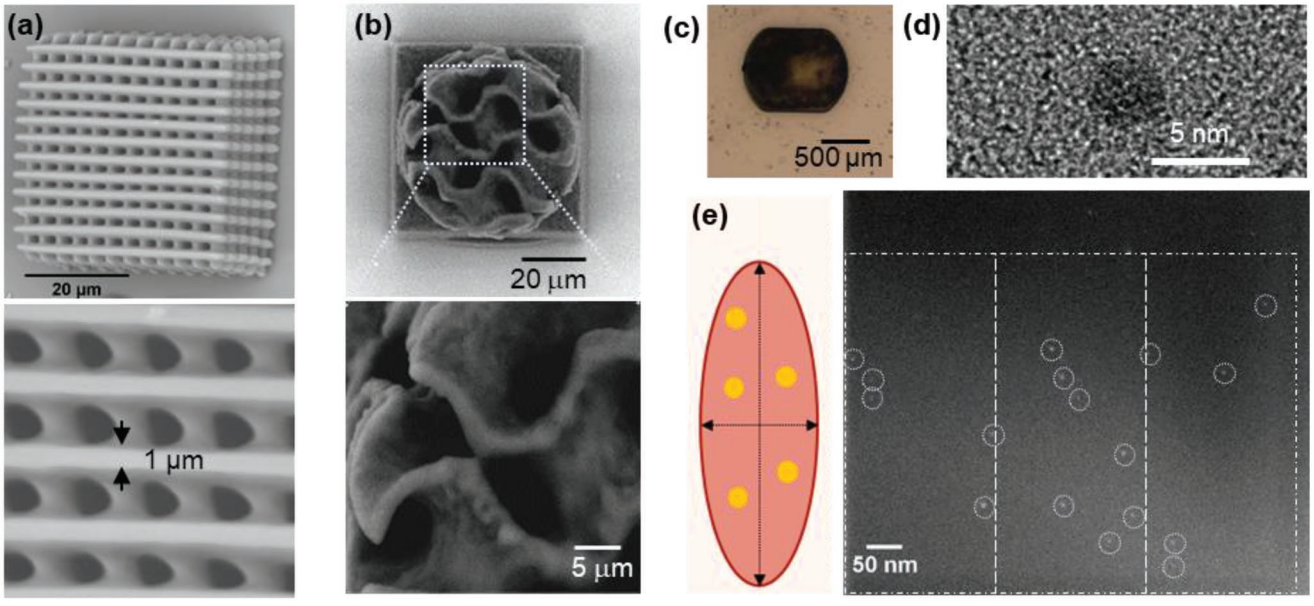

Figure 4. Direct 2PP with preformed AuNPs integrated into thiol-ene resins: a) SEM images of a woodpile structure (printing parameters: 10 mW and 15 mm s^{-1}) and b) a gyroid structure using Au-thiol-ene resin (printing parameters: 20 mW and 10 mm s^{-1}). c) Optical microscope image of 3D microstructure for cross section analysis using Au-thiol-ene resin (printing parameters: 35 mW and 10 mm s^{-1}). d) High-resolution TEM image of a AuNP within the 2PP structure. e) Cartoon of a voxel with calculated AuNPs density (5 AuNPs per a voxel) for 0.01 wt.% of AuNPs and TEM HAADF cross section image showing ≈ 6 AuNPs per 200 × 500 nm area equivalent to the voxel dimension.

Thus, the 2PP fabrication strategy developed here for integration of preformed NPs using thiol-functionalized resins offers significant advantages of uniformly sized NPs with pre-defined properties, which are well dispersed within the final structure. These results are of potential interest for (nano)-plasmonics and metamaterial applications. For example, it is envisaged that this strategy could be used in conjunction with other nanofillers, such as QDs,[32] CNTs[33] or magnetic particles,[34] to offer opportunities for tuning the composition of the 2PP structures with complex micro/nano-scaled designs. To fully unleash the potential of 2PP, the integration of (nano)material-containing parts into multimaterial structures and selective surface patterning with MeNPs need to be developed.

2.3. Multimaterial 2PP for the Selective Surface Decoration of 3D Microstructures with Metal Nanoparticles

A combination of 3D printing and electroless metal plating has been used to achieve the fabrication of surface coatings on entire 3D structures.[35,36] However, for applications requiring selective metal patterning, complex multistep processes are needed. This has limited the uptake of such techniques for site-specific metallic coating of complex surfaces. To overcome this issue, we proposed that 2PP multimaterial fabrication could provide surface functionality of intricate 3D structures via selective/patterned decoration with metal nanoparticles.

We employ 2PP-induced thiol-ene chemistry to introduce thiol functionality into the resin formulation, where thiols and reacted thioether functional groups are located on the surface of the built structure. It was envisaged that these moieties could then provide anchoring sites for MeNPs attachment due to affinity of metals, such as Au, to thiols (**Figure 5**a). Thus, 3D microstructures were fabricated using resins with different molar ratios of PETA:TrisSH. The polymerization threshold for 2PP-induced thiol-ene reaction (7.5 mW, 5 mm s^{-1}, 150 μJ $μm^{-3}$) was noted to be lower than that needed for the polymerization of PETA alone (15 mW, 5 mm s^{-1}, 300 μJ $μm^{-3}$). Hence, 2PP structures were successfully formed with lower laser powers. The FT-IR and XPS spectra of the resultant polymer structures reveal the formation of thioether bonds, hence confirming that thiols had participated in a 2PP-induced thiol-ene reaction (Figure S10, Supporting Information).

To assess the attachment of AuNPs to the surface of thiol-ene containing structure, the printed structure was immersed in a dispersion of AuNPs (40 wt.% in terpineol). Good adhesion between 2PP fabricated thiol-ene structure and AuNPs was confirmed by ToF-SIMS mapping. This showed strong Au signals on the printed surface (Figure 5b,c), which indicated that significant numbers of AuNPs were attached to the structures. Furthermore, structures produced with higher thiol-content resins exhibited greater Au signal intensities, with the response noted to increase by ≈60% when the thiol content was raised from 20% to 40%, (Figure S11, Supporting Information). To demonstrate

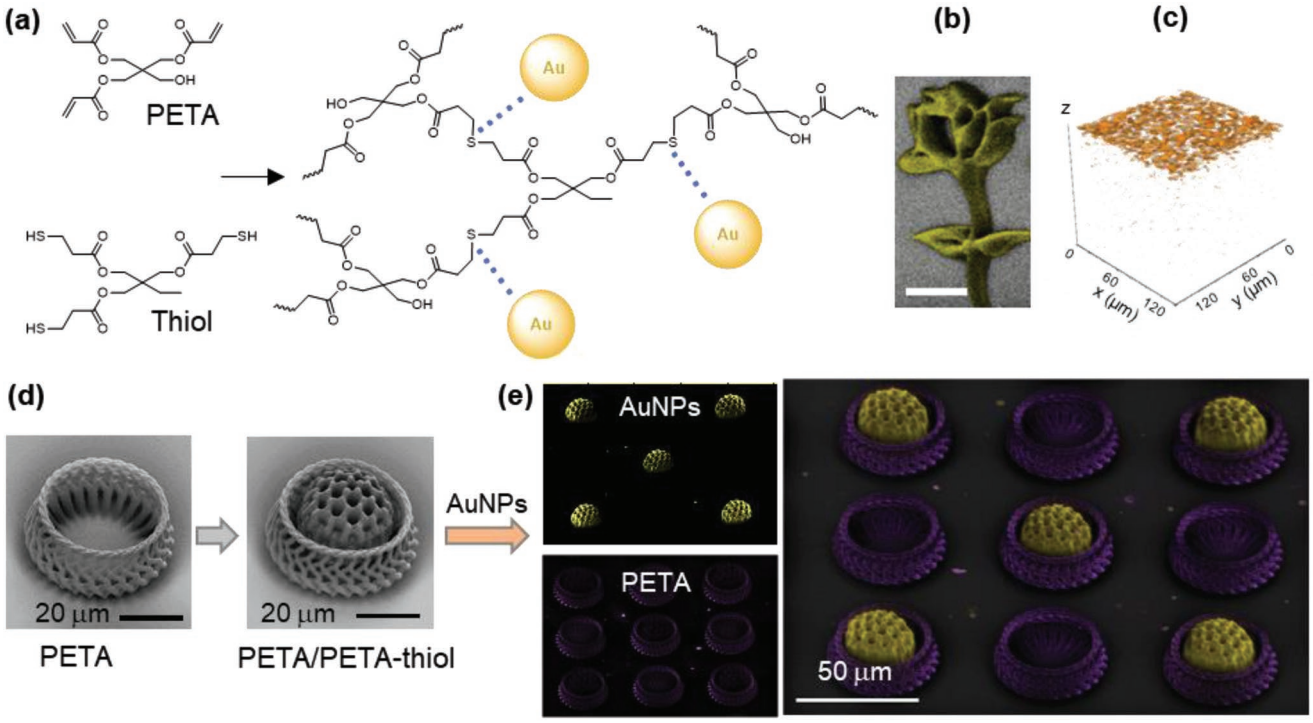

Figure 5. Site-selective Au decoration of 3D printed multimaterial structure: a) Chemical structures of the resins used and a schematic of selective Au deposition on 2PP thiol-ene structure. b) ToF-SIMS mapping analysis of Au for the printed thiol-ene polymer structure (yellow-Au_3^-, grey-SiO_2^-, scale bar 20 μm). c) 3D ToF-SIMS mapping of Au_3^- signal for the thiol-ene structure (PETA : TrisSH = 2:1) following 3 h immersion into AuNP solution (arbitrary depth scale). d) Printed multimaterial structures from acrylate resin formulation (PETA, printing parameter: 32.5 mW and 10 mm s^{-1}) and thiol-ene polymer (printing parameter: 20 mW and 10 mm s^{-1}). e) ToF-SIMS mapping images of the 3D multimaterial structures with selective AuNPs surface decoration. Au-related signal map is shown in yellow and PETA-related signal map is shown in purple

site-selective nature of the Au decoration, multimaterial structures consisting of the parts printed using PETA-only resin and thiol-ene resin (Figure 5d) were fabricated. Immersion of these multimaterial structures in the dispersion of AuNPs resulted in selective NP attachment to thiol-containing parts only. Non-negative matrix factorization of ToF-SIMS data revealed that the Au signals (Figure 5e, Figure S11, Supporting Information) were detected exclusively on the surface of bucky-ball fabricated using thiol-ene resin. It was found that the longer immersion time increases the amount of AuNPs attached onto the thiol-ene structure and the depth of AuNP penetration, as revealed by the ToF-SIMS depth profile images (Figure S12, Supporting Information). This data suggested the presence of thiol and thioether both on the surface and within the volume of the printed structure and confirmed the role of the thiol/thioether functionality in achieving the selectivity of attachment for the AuNP decoration. 2PP with thiol-ene and thiol-yne resins have been used to build 3D mesostructures[37] and thiol functionality is also known to have high affinity to metal nanoparticles such as AuNPs.[38] Here we demonstrate that multimaterial 2PP with PETA and thiol-ene resins offer a route for fabrication of intricate geometries with sub-micron resolution as well as to achieve selective decoration of complex and curved surfaces. This facile methodology for selective Au patterning of micro/nanoscale surfaces, including curved and intricately designed surfaces, opens up new opportunities for micro/nano plasmonic metal patterns for applications such as sensing and metamaterials.

3. Conclusions

Three novel strategies, with complementary capabilities, to achieve the integration/dispersion of MeNPs with 2PP processing have been developed. Furthermore, successful fabrication of high-fidelity structures with incorporated MeNPs has been demonstrated. A method involving simultaneous photopolymerization and photoreduction method was shown to offer flexibility for the incorporation of MeNPs into 3D structures. In this strategy, the loading of NPs was tuneable by varying metal salt concentrations. Additionally, this strategy is transferable to different metal salts, e.g. AuNPs, AgNPs, and CuNPs. Meanwhile, precise control of the NP size, shape, and composition within the 2PP structures was successfully achieved by formulating a resin containing preformed NPs with both photoreactive monomers and a thiol-functionality. In both strategies, the NPs are embedded within the volume of the fabricated structures, and the quality of the dispersion was much improved by the use of the preformed NPs. For selective decoration and patterning of the 3D surfaces, a multimaterials 2PP methodology was developed to fabricate 3D structures containing both PETA-only parts and the thiol-ene resin parts. This generated 3D-built structures with thiols and thioethers, which have high affinity to metal centers, located both in the bulk and at the surface. This allows high degree of selectivity and the level of metal decoration controllable by the concentration of thiols in the resin and the duration of the immersion. These complementary strategies open up a broad range of prospective applications from metamaterials and nano/micro-photonics to optoelectronics and biomedicine and merit further detailed studies.

4. Experimental Section

Materials: Pentaerythritol triacrylate (PETA, Sigma-Aldrich) and trimethylolpropane tri(3-mercaptopropionate) (TrisSH, Sigma-Aldrich) were used as monomers. 2-Benzyl-2-(dimethylamino)-4′-morpholinobutyrophenone (Irgacure 369, Sigma-Aldrich) and 7-diethylamino-3-thenoylcoumarin (DETC, Angene International) were used as PI and Coumarin 30 (Sigma-Aldrich) was employed as a photosensitive dye. Silver nitrate (Sigma-Aldrich) and copper sulfate (Sigma-Aldrich) were used as the metal salts and toluene (Sigma-Aldrich) was chosen as a solvent for extracted silver and copper ions, PETA and Coumarin 30. Dodecylamine (DDA, Sigma-Aldrich) and ethanol (Sigma-Aldrich) were used to help transfer silver nitrate from water to toluene.

Phase-Transfer Protocol: To prepare the silver-polymer nanocomposites for 2PP fabrication, the silver ions were transferred from water to toluene. One milliliter of 0.5 M aqueous silver nitrate solution was mixed with 1 mL of ethanol containing DDA with the mole ratio of DDA: silver nitrate of 10:1. After 5 min stirring, 1 mL of toluene was added and the stirred for another 5 min. The final concentration of silver in toluene is 0.5 M. Then, 1, 3, and 5 wt.% of Irgacure 369 were added to PETA separately. Silver ions (0.5 M) in toluene with the 1:5 molar ratio of silver ions: PETA and 0.1 wt.% Coumarin 30 as a photosensitive dye were added to the photoresist (Table 1). The resins were mixed using a magnetic stirrer for 30 min at 600 rpm.

To prepare the resin formulation for a copper-polymer nanocomposite, 1 mL of 0.3 M aqueous copper (II) sulfate pentahydrate solution[23] was mixed with 1 mL of ethanol containing DDA with the 10:1 mole ratio of DDA: copper (II) sulfate pentahydrate and stirred for 5 min. Then 1 mL of toluene was added and the mixture was stirred for 5 min. The copper ions in toluene were transferred into toluene. Next, 5 wt.% of Irgacure 369 was added to PETA. Formulation with Coumarin 30 was prepared as described above (see Table 1).

Resin Formulation with Pre-Formed NPs with 2PP: Octanethiol-functionalized gold nanoparticles (OT-AuNPs) were synthesized by the method described in the previous publication.[39] OT-AuNPs were dispersed in terpineol (mixture of isomers) and then mixed with PETA and TrisSH (1:1 weight ratio) and DETC (0.2 wt.%) with varying concentrations of OT-AuNPs ranging from 0 to 1 wt.%. The mixture was sonicated using a bath sonicator for 30 min and then stirred overnight.

Sample Preparation for Selective Surface Decoration with AuNPs: The resin for 2PP was prepared by mixing two monomers, PETA and TrisSH, with different molar ratios of 5:1 and 2:1 and DETC (0.2 wt.%). The mixture was stirred overnight before printing. The 3D microstructures fabricated by 2PP was decorated with AuNPs by placing a droplet of the dispersion of OT-AuNPs (40 wt.%) in terpineol on the surface of the 3D structure for different decoration time and rinsing it with terpineol and then isopropanol after decoration.

Multiphoton Fabrication: A commercial two-photon lithography system (Nanoscribe GmbH Photonic Professional GT) was used for the multiphoton fabrication. The system was equipped with a fiber laser at a central wavelength of 780 nm, 80 MHz repetition rate, and 120 fs pulse duration. The laser beam was focused using an oil immersion objective lens (63 ×, NA = 1.4, WD = 190 µm). 3D micro/nanostructures were fabricated by moving the sample position in the XY plane using a galvo scanner and in the *z*-direction using a piezoelectric actuator to move the objective. The laser power and scan speed varied between 10 and 50 mW and between 10 and 21 mm s^{-1}, respectively. After printing, the samples were developed using propylene glycol monomethyl ether acetate (PGMEA) for 15 min and washed further with 2-propanol for 5 min to remove residual resin. The resin preparation and two-photon fabrication were carried out in UV-free environment. The energy density was calculated from the following equation:

$$E = \frac{P}{\upsilon \cdot h \cdot t} \tag{1}$$

where P, υ, h, and t are the laser power, scan speed, hatching distance, and layer thickness, respectively.[40]

Characterization Methods: Optical microscopy images were acquired using an optical microscope (Nikon Eclipse LV100ND). Scanning electron microscopy (SEM) was used to obtain the morphology of printed samples (Philips XL30, Philips, UK, and Hitachi TM3030). Energy-dispersive X-ray spectroscopy (EDX) (Philips XL30, Philips, UK), X-ray photoelectron spectroscopy (XPS) (Kratos Axis Ultra DLD, Kratos Analytical Ltd, France), and Raman spectroscopy (Horiba-Jobin-Yvon LabRAM, Horiba-Jobin-Yvon, France) were used to perform chemical analysis. The degree of vinyl group consumption (*DC*) was assessed as the proportion of reacted vinyl groups using the following equation:

$$DC = \left[1 - \left(\frac{A_{C=C}/A_{C=O}}{A'_{C=C}/A'_{C=O}}\right)\right] \times 100\% \quad (2)$$

where $A_{C=C}$, $A_{C=O}$, and $A'_{C=C}$, $A'_{C=O}$ are the integrated Raman peak intensities related to the C=C (1638 cm^{-1}) and C=O (1726 cm^{-1}) bonds in the polymerized structures and the non-polymerized monomers, respectively.

Cross sections of the polymerized samples were prepared using Quanta 200 3D (FEI Company, Hillsboro, Oregon, USA) and Crossbeam 550 (Carl Zeiss, Oberkochem, Germany) FIB-SEMs and extracted using an Omniprobe Micromanipulator (Oxford Instruments, Abingdon, Oxfordshire, UK). JEOL 7100F FEG-SEM (field emission gun scanning electron microscopy) (JEOL, Nieuw-Vnnep, Amsterdam) and JEOL 2100F FEG-TEM (field emission gun transmission electron microscope) (JEOL, Amsterdam) were used to characterize nanoparticles within polymer matrix. Perkin Elmer Optima 2000 ICP-OES (Inductively coupled plasma atomic emission spectroscopy) instrument (Perkin Elmer, United States) was employed to measure the phase transfer efficiency of silver ions.

ToF-SIMS mapping of 2PP structures was carried out using a 3D OrbiSIMS (Hybrid SIMS) instrument from IONTOF GmbH. The ToF-SIMS data were acquired in negative and positive ion polarity mode in delayed extraction mode by raster scanning a 30 keV Bi_3^+ primary ion beam delivering 0.08 pA and a low-energy (20 eV) electron flood gun employed to neutralize charge build-up. Depth profiles were obtained with an argon gas cluster ion beam (GCIB) operated with 10 keV and 1500 atoms in the cluster with 3 nA beam current. Unsupervised machine learning was carried out using the mass as the variables and mapping pixels as observations. For each dataset, Surface Lab 7.1 (IONTOF GmbH) was used to perform an automated peak search on the total spectra. Peak areas were then exposed for each pixel. Data were Poisson scaled to account for heteroscedasticity[41] and non-negative matrix factorization was performed using the simsMVA software.[42]

Statistical Analysis: All representative experimental results presented in the Figures are shown as measured. All measurements were performed with a minimum of three independent replicates and the results are shown as mean ± SD.

Supporting Information

Supporting Information is available from the Wiley Online Library or from the author.

Acknowledgements

J.I. and Y.L. contributed equally to this work. This work was funded by the Engineering and Physical Sciences Research Council [grant number EP/P031684/1] and USAF EOARD award [grant number FA9550-17-1-0186]. Access to analytical instruments and facilities was funded by Engineering and Physical Sciences Research Council strategic equipment grant [grant number EP/P029868/1] (3D orbiSIMS facilities), [EP/S021434/1] (FIB-SEM) and [EP/L011883/1] (SEM and TEM). The authors acknowledged access to the facilities at the Nanoscale and Microscale Research Centre and assistance with measurement from Dr Emily Smith for XPS and Dr Graham Rance for Raman studies.

Conflict of Interest

The authors declare no conflict of interest.

Data Availability Statement

The data that support the findings of this study are available from the corresponding author upon reasonable request.

Keywords

gold nanoparticles, metal nanoparticles, micro additive manufacturing, multi-material printing, silver nanoparticles, Two-photon polymerization

Received: October 14, 2022
Revised: November 27, 2022
Published online:

[1] A. Camposeo, L. Persano, M. Farsari, D. Pisignano, *Adv. Opt. Mater.* **2019**, *7*, 1800419.
[2] R. D. Sochol, E. Sweet, C. C. Glick, S.-Y. Wu, C. Yang, M. Restaino, L. Lin, *Microelectron. Eng.* **2018**, *189*, 52.
[3] A. S. Cordeiro, I. A. Tekko, M. H. Jomaa, L. Vora, E. McAlister, F. Volpe-Zanutto, M. Nethery, P. T. Baine, N. Mitchell, D. W. McNeill, R. F. Donnelly, *Pharm. Res.* **2020**, *37*, 174.
[4] S. A. M. Tofail, E. P. Koumoulos, A. Bandyopadhyay, S. Bose, L. O'Donoghue, C. Charitidis, *Mater. Today* **2018**, *21*, 22.
[5] F. Kotz, A. S. Quick, P. Risch, T. Martin, T. Hoose, M. Thiel, D. Helmer, B. E. Rapp, *Adv. Mater.* **2021**, *33*, 2006341.
[6] V. Harinarayana, Y. C. Shin, *Opt. Laser Technol.* **2021**, *142*, 107180.
[7] M. Carlotti, V. Mattoli, *Small* **2019**, *15*, 1902687.
[8] L. Yang, F. Mayer, U. H. F. Bunz, E. Blasco, M. Wegener, *Light* **2021**, *2*, 296.
[9] S. Shukla, X. Vidal, E. P. Furlani, M. T. Swihart, K. T. Kim, Y. K. Yoon, A. Urbas, P. N. Prasad, *ACS Nano* **2011**, *5*, 1947.
[10] E. Blasco, J. Muller, P. Muller, V. Trouillet, M. Schon, T. Scherer, C. Barner-Kowollik, M. Wegener, *Adv. Mater.* **2016**, *28*, 3592.
[11] I. Sakellari, X. Yin, M. L. Nesterov, K. Terzaki, A. Xomalis, M. Farsari, *Adv. Opt. Mater.* **2017**, *5*, 1700200.
[12] R. Momper, A. I. Landeta, L. Yang, H. Halim, H. Therien-Aubin, E. Bodenschatz, K. Landfester, A. Riedinger, *ACS Appl. Mater. Interfaces* **2020**, *12*, 50834.
[13] W.-E. Lu, Y.-L. Zhang, M.-L. Zheng, Y.-P. Jia, J. Liu, X.-Z. Dong, Z.-S. Zhao, C.-B. Li, Y. Xia, T.-C. Ye, X.-M. Duan, *Opt. Mater. Express* **2013**, *3*, 1660.
[14] Y. Liu, Q. Hu, F. Zhang, C. Tuck, D. Irvine, R. Hague, Y. He, M. Simonelli, G. A. Rance, E. F. Smith, R. D. Wildman, *Polymers* **2016**, *8*, 325.
[15] Q. Hu, X. Z. Sun, C. D. J. Parmenter, M. W. Fay, E. F. Smith, G. A. Rance, Y. He, F. Zhang, Y. Liu, D. Irvine, C. Tuck, R. Hague, R. Wildman, *Sci. Rep.* **2017**, *7*, 17150.
[16] S. K. Saha, B. Au, J. S. Oakdale, *Adv. Eng. Mater.* **2019**, *21*, 1900583.
[17] M. Focsan, A. M. Craciun, S. Astilean, P. L. Baldeck, *Opt. Mater. Express* **2016**, *6*, 1587.
[18] W.-S. Kuo, C.-H. Lien, K.-C. Cho, C.-Y. Chang, C.-Y. Lin, L. L. H. Huang, P. J. Campagnola, C. Y. Dong, S.-J. Chen, *Opt. Express* **2010**, *18*, 27550.
[19] K. Masui, S. Shoji, K. Asaba, T. C. Rodgers, F. Jin, X.-M. Duan, S. Kawata, *Opt. Express* **2011**, *19*, 22786.
[20] S. Shukla, E. P. Furlani, X. Vidal, M. T. Swihart, P. N. Prasad, *Adv. Mater.* **2010**, *22*, 3695.

[21] R. Nakamura, K. Kinashi, W. Sakai, N. Tsutsumi, *Phys. Chem. Chem. Phys.* **2016**, *18*, 17024.
[22] J. Yang, E. H. Sargent, S. O. Kelley, J. Y. Ying, *Nat. Mater.* **2009**, *8*, 683.
[23] Q. Hu, G. A. Rance, G. F. Trindade, D. Pervan, L. Jiang, A. Foerster, L. Turyanska, C. Tuck, D. J. Irvine, R. Hague, R. D. Wildman, *Addit. Manuf.* **2022**, *51*, 102575.
[24] A. Ishikawa, T. Tanaka, S. Kawata, *Appl. Phys. Lett.* **2006**, *89*, 113102.
[25] E. H. Waller, G. v. Freymann, *Nanophotonics* **2018**, *7*, 1259.
[26] S. Tabrizi, Y. Y. Cao, H. Lin, B. Jia, *Sci. China Phys. Mech.* **2017**, *60*, 034201.
[27] K.-W. Yeung, Y. Dong, L. Chen, C.-Y. Tang, W.-C. Law, G. C.-P. Tsui, D. S. Engstrom, *Nanotechnol. Rev.* **2020**, *9*, 418.
[28] A. K. O'Brien, N. B. Cramer, C. N. Bowman, *J. Polym. Sci., Part A: Polym. Chem.* **2006**, *44*, 2007.
[29] L. Jiang, W. Xiong, Y. Zhou, Y. Liu, X. Huang, D. Li, T. Baldacchini, L. Jiang, Y. Lu, *Opt. Express* **2016**, *24*, 13687.
[30] M. E. Whitely, J. L. Robinson, M. C. Stuebben, H. A. Pearce, M. A. P. McEnery, E. Cosgriff-Hernandez, *ACS Biomater. Sci. Eng.* **2017**, *3*, 409.
[31] J. Fischer, M. Wegener, *Laser Photonics Rev.* **2013**, *7*, 22.
[32] Y. Peng, S. Jradi, X. Yang, M. Dupont, F. Hamie, X. Q. Dinh, X. W. Sun, T. Xu, R. Bachelot, *Adv. Mater. Technol.* **2019**, *4*, 1800522.
[33] W. Xiong, Y. Liu, L. J. Jiang, Y. S. Zhou, D. W. Li, L. Jiang, J. F. Silvain, Y. F. Lu, *Adv. Mater.* **2016**, *28*, 2002.
[34] H. Xia, J. Wang, Y. Tian, Q. D. Chen, X. B. Du, Y. L. Zhang, Y. He, H. B. Sun, *Adv. Mater.* **2010**, *22*, 3204.
[35] K.-M. Huang, S.-C. Tsai, Y.-K. Lee, C.-K. Yuan, Y.-C. Chang, H.-L. Chiu, T.-T. Chung, Y.-C. Liao, *RSC Adv.* **2017**, *7*, 51663.
[36] S. Lee, M. Wajahat, J. H. Kim, J. Pyo, W. S. Chang, S. H. Cho, J. T. Kim, S. K. Seol, *ACS Appl. Mater. Interfaces* **2019**, *11*, 7123.
[37] A. S. Quick, A. d. l. S. Pereira, M. Bruns, T. Bückmann, C. Rodriguez-Emmenegger, M. Wegener, C. Barner-Kowollik, *Adv. Funct. Mater.* **2015**, *25*, 3735.
[38] B. Buchegger, C. Vidal, J. Neuwirth, B. Buchroithner, A. Karner, A. Hochreiner, T. A. Klar, J. Jacak, *ACS Mater. Lett.* **2019**, *1*, 399.
[39] J. Im, G. F. Trindade, T. T. Quach, A. Sohaib, F. Wang, J. Austin, L. Turyanska, C. J. Roberts, R. Wildman, R. Hague, C. Tuck, *ACS Appl. Nano Mater.* **2022**, *5*, 6708.
[40] L. Thijs, F. Verhaeghe, T. Craeghs, J. V. Humbeeck, J. -P. Kruth, *Acta Mater.* **2010**, *58*, 3303.
[41] M. R. Keenan, P. G. Kotula, *Surf. Interface Anal.* **2004**, *36*, 203.
[42] G. F. Trindade, M.-L. Abel, J. F. Watts, *Chemom. Intell. Lab. Syst.* **2018**, *182*, 180.